OPTIMIZATION OF DISK GENERATOR PERFORMANCE FOR BASE-LOAD POWER PLANT SYSTEMS APPLICATIONS

J.D. Teare, W.J. Loubsky, J.K. Lytle, J.F. Louis

Massachusetts Institute of Technology
Cambridge, MA 02139

CONF-800617--6

Abstract

Disk generators for use in base-load MHD power plants are examined for both open-cycle and closed-cycle operating modes. The OCD cases are compared with PSPEC results for a linear channel; enthalpy extractions up to 23% with 71% isentropic efficiency are achievable with generator inlet conditions similar to those used in PSPEC, thus confirming that the disk configuration is a viable alternative for base-load power generation. The evaluation of closed-cycle disks includes use of a simplified cycle model. High system efficiencies over a wide range of power levels are obtained for effective Hall coefficients in the range 2.3 to 4.9. Cases with higher turbulence (implying $\beta_{eff} \leq 2.4$) yield high system efficiencies at power levels of 100-500 MW_e. All these CCD cases compare favorably with linear channels reported in the GE ECAS study, yielding higher isentropic efficiences for a given enthalpy extraction. Power densities in the range 70-170 MW/m^3 appear feasible, leading to very compact generator configurations.

I. Introduction

The potential of a disk generator with swirl as an alternative to a linear channel for high performance MHD power generation has received considerable attention[1-5] in recent years. The attractiveness of the disk configuration is enhanced by (a) the inherent advantages (such as single load capability) arising from the circular symmetry, (b) encouraging laboratory results from shock tunnel experiments, and (c) the expected simplicity and lower cost of the superconducting magnet system. Under a NASA contract with Westinghouse, a systems study is being carried out to determine overall performance capabilities for coal-fired power plants using disk generators in either open-cycle or closed-cycle mode. The present paper discusses the methodology and results of M.I.T. work to optimize the performance of the disk generator itself, subject to constraints imposed by the rest of the power plant components and by physical limitations within the generator subsystem (e.g., maximum permissible electric field, diffuser recovery coefficient, and generator inlet losses).

The paper first addresses the OCD generator optimization, with a brief review of the model and of the significant cycle parameters, such as electrical and isentropic efficiency and enthalpy extraction capability. The appropriate constraints for the OCD design are then examined, and the potential performance of a disk generator with 2000 MW_{th} input is assessed. An obvious figure-of-merit for such performance is derivable from comparison with the expected performance of equivalent open-cycle linear generators, with the results of the Avco PSPEC study[6] being most appropriate. Although PSPEC and the Westinghouse-MIT studies call for very similar oxidizer preheat and combustor exit conditions, the head-to-head comparison would not be valid unless the plasma conditions were truly equivalent; since Ref. 6 does not give specific conductivity values, the present results are discussed parametrically in terms of a conductivity enhancement factor. The disk optimization procedures are applied for both single-load and multi-load configurations, and an overall comparison with PSPEC is given.

The closed-cycle nonequilibrium disk MHD generator is characterized (relative to the OCD) by high interaction and compactness. The circular symmetry/configuration of the outward-flow generator provides high inlet dissipation with a consequent short ionization relaxation length relative to the linear closed-cycle counterpart[2]. As a result, performance and potential cost benefits may be realized with a CCD system. Performance optimization in the CCD case, however, is more complex because of the additional parameters which control the conductivity/interaction. In the paper the generator model formulation and local performance characteristics of the CCD are reviewed. The optimization procedure is outlined and example results which suggest the potential viability of the CCD system are discussed.

II. Open-Cycle Disk Generator Optimization

Generator Model and Assumptions

The modeling has been restricted to a quasi-one-dimensional description of the channel flow, with the effects of wall friction and heat loss being averaged over the channel height at each radial station. The OCD working fluid is obtained from direct combustion of coal in preheated air (or air with O_2 enrichment). The plasma properties are characterized by the pressure and enthalpy of this working fluid, with equilibrium conductivity($T_e = T$) being assumed.

The basic fluid dynamical conservation equations for a disk are given in Figure 1. Cylindrical polar coordinates are used, with the magnetic field aligned with the z-axis. Local values of current densities and short-circuit radial current density can be expressed in terms of electrical conductivity, σ, Hall parameter, β, and swirl ratio, S. Local electrical efficiency depends on the load factor, K, attaining a maximum at an optimum load factor which is a simple function of β and S. When $K \neq K_{opt}$ the degradation of local efficiency depends solely on the values of K and K_{opt}. From the expression for dh_o/dr an enthalpy extraction length can be derived, and this is clearly minimized by selecting $K = 0.5$. Thus the disk optimization procedure centers on achieving a compromise between maximizing the rate of enthalpy extraction and maintaining local electrical efficiency as high as possible. One of the important parameters affecting this compromise is the maximum permissible value of radial electric field.

A high-performance disk generator must undoubtedly withstand very much higher Hall fields than an equivalent linear generator, but the technological problems associated with an insulating wall are somewhat different from those of electrode wall construction. Fields in excess of 30 kV/m have been measured without any indication of breakdown in shock tube experiments with cold walls. There are no relevant experimental data for the hot wall situation, but it is conceivable that no appreciable decrease in breakdown voltage will occur until the wall temperature exceeds ~2200 K. For $\beta \geq 3$ it can be argued that a field of magnitude βE_x over an insulating wall leads to the same Joule dissipation as a field E_x over an electrode wall. Thus an insulator wall should be capable of sustaining (before breakdown) an electric field β times larger than an electrode wall, and this is consistent with linear generator experience. Using this rationale, a maximum Hall field constraint of 12 kV/m was adopted for the disk systems analysis base cases.

Throughout the open-cycle section of this paper it is assumed that the magnetic field is 7 Tesla, originally selected to be within the state-of-the-art for Nb-Ti, but certainly well within the capabilities of the more recently developed Nb_3-Sn technology.

Stagnation conditions at the combustor exit have been taken to be $T_o = 2579$ K and $P_o = 8.3$ atm, consistent with values used in one of the PSPEC base

Conservation Equations:

$$\rho u_r \frac{du_r}{dr} + \frac{dp}{dr} = \frac{\rho u_\theta^2}{r} + j_\theta B - \frac{\rho u u_r f}{z}$$

$$\rho u_r \frac{du_\theta}{dr} = -\frac{\rho u_r u_\theta}{r} - j_r B - \frac{\rho u u_\theta f}{z}$$

$$\rho u_r \frac{d}{dr}\left(h + \frac{u_r^2 + u_\theta^2}{2}\right) = j_r E + \frac{2}{z}\dot{Q}$$

where $f = 0.0576\,[Re]^{-0.2}$, $\dot{Q} = \rho u\,[St](h_{aw} - h_w)$

and $[St] = 0.0295\,[Re]^{-0.2}[Pr]^{-0.4}$

Electrical Behavior:

$$j_r = \frac{I_{load}}{2\pi rz}, \qquad j_{rsc} = \frac{\sigma(\beta+S)u_r B}{(1+\beta^2)}, \qquad K = \frac{j_r}{j_{rsc}}$$

$$j_\theta = \beta j_r - \sigma u_r B \qquad \text{and} \qquad E = -(1-K)(\beta+S)u_r B$$

Electrical Efficiency:

$$\eta_L = \frac{(\beta+S)^2 K(1-K)}{(1+\beta^2) - (\beta^2 - S^2)K}, \qquad K_{opt} = \frac{\beta_1}{\beta_1 + S_1}$$

where $\beta_1^2 = 1 + \beta^2$ and $S_1^2 = 1 + S^2$

$$\eta_{L(max)} = \left(\frac{\beta+S}{\beta_1+S_1}\right)^2 \quad \text{and} \quad \frac{\eta_L}{\eta_{L(max)}} = \frac{K(1-K)}{K(1-K) + (K-K_{opt})^2}$$

Enthalpy Extraction Length:

$$\frac{dh_o}{dr} = \frac{j_r E}{\rho u_r} = -\frac{K(1-K)(S+\beta)^2 \sigma u_r B^2}{\rho(1+\beta^2)} + \frac{\Delta h_o}{L_{ex}}$$

$$L_{ex}(K) = \frac{\rho \Delta h_o}{\sigma u_r B^2}\,\frac{(1+\beta^2)}{K(1-K)(S+\beta)^2}, \qquad L_{ex}(K_{opt}) = \frac{\rho \Delta h_o}{\sigma u B^2}\,\frac{\beta_1}{\eta_{L(max)}}$$

Figure 1. Disk Model and Local Performance Parameters.

cases and attainable with air preheated to 1920 K (3000°F). In Ref. 6 these values are defined as the linear generator inlet conditions; however, the need for relatively high swirl at the inlet to the disk generator would almost certainly incur additional losses. It has been assumed that swirl ratios up to 0.5 could be attained with a high swirl second-stage combustor, but that higher swirl would dictate the use of inlet guide vanes (IGVs). In some of the cases discussed, the added penalties due to IGVs are modeled as $\Delta P_o = 0.025(S-0.5)$ and $\Delta h_o = 0.01(S-0.5)$.

Most of the Westinghouse-MIT studies have been based on potassium seeding of 0.7% by weight: the σ-β values for this plasma were calculated by B. Lu using the NASA LeRC code, and they are consistent with values reported at the 1979 DOE Workshop.[7] Dr. Lu's values, identified as $\sigma_{0.7}$, are treated as the 'basic' values in the present paper. The PSPEC calculations, on the other hand, use 1% K-seeding, which would normally produce at most a 19% increase in conductivity. Conductivity levels are not published in Ref. 6, but there are sufficient data presented to enable σ-values in the generator core flow to be deduced. The published values of channel pressure yield j_y from $dp/dx = j_y B$, and this can be used with the published E_{xc}, E_{yc} and β to yield σ_c directly. Within the core of the appropriate channel the deduced values indicate $\sigma_c/\sigma_{0.7} \sim 1.6$. However, more recent data furnished to NASA LeRC by Avco indicate levels of $\sigma_{Avco}/\sigma_{0.7} \sim 1.3$. Thus the present report includes results of channel calculations in which a multiplicative "σ-factor" of 1.0, 1.33 or 1.6 is applied throughout the active region of the generator.

Finally, the modeling requires a stipulation of channel exit conditions, and here again the choice is consistent with PSPEC, exhausting to a diffuser with a recovery coefficient of 0.6 and exit total pressure of 1 atm. Since all the disk cases shown are supersonic, it is assumed that a normal shock will occur at entry to the axisymmetric diffuser.

Design constraints and optimization results

When all inlet conditions to the disk generator (mass flow rate; stagnation conditions, P_o, T_o; Mach number, M; swirl ratio, S; and load factor, K) are preselected, it is still necessary to apply one constraint before the fluid and electrical properties throughout the generator can be calculated. This constraint is equivalent to choice of impulse mode, reaction mode or a combination of both; it may be effected, for example, by specification of dT/dr, dh/dr or M as a function of radial position. A significant advance came with the recognition that use of the electric-field constraint is an effective way to force a type of suboptimization in the sense that it permits direct comparisons of the results of design calculations for different choices of the inlet values of P_o, M or S. By choosing the initial load factor, K, to make $E = -(1-K)Bu_r(S+\beta)$ assume the maximum value permitted by the design specification, and by subsequently controlling dh/dr to maintain the E-field at this maximum value, it is possible to obtain a generator which is more compact than any other design having the same initial conditions and the same electrical power output. Parametric variations of P_o, M and S can then be made to provide an optimum choice within the family of constant E-field designs.

As would be expected, the optimum inlet pressure is determined by overall cycle considerations, and is primarily dependent on the maximum enthalpy extraction attainable. The variation of performance with choice of inlet M and S is exemplified in Figure 2. These curves are developed for a substantially lower stagnation temperature ($T_o \sim 2834$ K), so that the maximum enthalpy extraction is only ~ 19%, and the optimum inlet pressure is between 6 and 7 atm. The figure shows variation of gross output power plotted against generator exit radius for a number of inlet M,S combinations. The beneficial effect of adding swirl is apparent until S ~ 0.5, but thereafter the gain from further increase in swirl is minimal, and probably offset by increased heat losses as the generator grows in size. The electrical efficiency increases with increasing M, and with increasing S at a

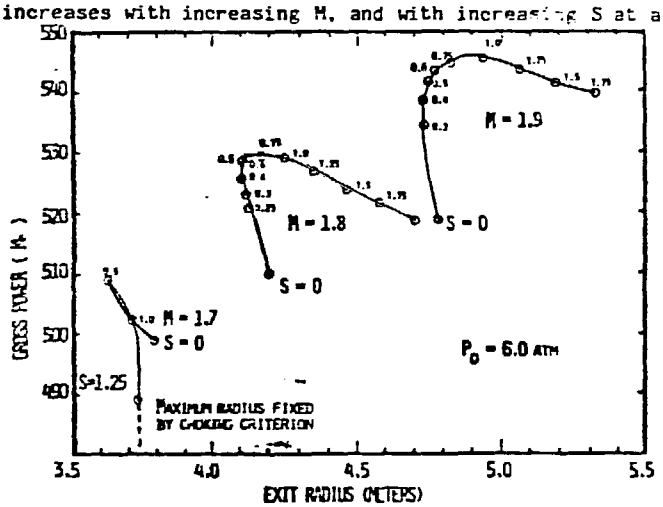

Figure 2. Gross Power vs Exit Radius as Functions of Inlet Mach Number and Swirl Ratio: Single-load. P_o=6 atm., T_o=2834 K, B=7 T, $\sigma=\sigma_{0.7}$

Table 1. Single-load Generator Characteristics. B = 7T, T_o = 2879 K, P_o = 8 atm.

A. Constraint: E = -12 kV/m

$\sigma/\sigma_{0.7}$ = 1.0

INLET S	INLET M	RMAX (m)	NET P (MW)	POWER (MW)	HT.LOSS (MW)	ENTH. EXTR.	ISEN EFFCY	ELEC EFFCY
0.50	1.70	4.747	455.03	629.06	46.45	21.13	63.85	67.44
1.00	1.70	4.653	440.83	614.86	47.02	20.65	64.17	67.45
1.50	1.70	4.590	399.18	573.21	49.47	19.26	64.21	67.86
2.00	1.70	4.691	374.12	548.15	51.86	18.41	64.42	68.56
0.50	1.80	5.208	467.58	641.59	51.86	21.55	64.98	69.59
1.00	1.80	5.193	462.38	636.42	54.03	21.38	65.69	70.15
1.50	1.80	5.268	442.35	616.38	56.68	20.70	66.02	70.78
2.00	1.80	5.374	418.78	592.82	59.24	19.91	66.21	71.50
0.50	1.90	5.823	479.95	653.98	60.59	21.97	65.88	72.31
1.00	1.90	5.886	479.91	653.94	63.08	21.97	66.96	73.00
1.50	1.90	6.180	475.26	649.28	66.72	21.81	67.42	74.10
2.00	1.90	6.429	468.83	642.86	70.61	21.60	67.61	74.78

$\sigma/\sigma_{0.7}$ = 1.6

INLET S	INLET M	RMAX (m)	NET P (MW)	POWER (MW)	HT.LOSS (MW)	ENTH. EXTR.	ISEN EFFCY	ELEC EFFCY
0.50	1.70	3.418	477.87	852.00	25.38	21.00	66.21	68.36
1.00	1.70	3.383	457.95	831.98	26.57	21.23	66.87	69.00
1.50	1.70	3.388	413.03	787.06	27.81	19.72	67.38	69.77
2.00	1.70	3.803	386.53	760.58	29.47	18.83	67.88	70.64
0.50	1.80	3.743	493.12	867.15	28.29	22.41	67.57	70.39
1.00	1.80	3.788	488.08	863.11	30.04	22.27	68.79	71.52
1.50	1.80	3.857	460.71	834.74	31.79	21.32	69.47	72.50
2.00	1.80	3.981	436.07	810.10	33.82	20.49	69.86	73.40
0.50	1.90	4.248	510.12	884.15	33.06	22.88	69.06	72.91
1.00	1.90	4.352	513.51	887.54	35.10	23.10	70.52	74.40
1.50	1.90	4.545	510.76	884.79	37.71	23.00	71.33	75.43
2.00	1.90	4.782	507.43	881.46	40.45	22.89	71.79	76.20

B. Constraint: K/K_{opt} = constant

INLET S	INLET M	RMAX (m)	NET P (MW)	POWER (MW)	HT.LOSS (MW)	ENTH. EXTR.	ISEN EFFCY	ELEC EFFCY
0.50	1.70	4.749	454.99	629.02	46.50	21.13	63.85	67.44
1.00	1.70	4.828	450.96	624.99	51.58	20.99	64.76	68.48
1.50	1.70	4.882	422.21	596.24	54.37	20.03	65.24	69.29
2.00	1.70	5.030	399.91	573.94	55.87	19.28	65.45	69.83
0.50	1.80	5.482	470.71	644.74	55.45	21.66	65.21	70.25
1.00	1.80	5.840	470.83	644.86	62.60	21.65	66.37	71.72
1.50	1.80	6.093	468.17	642.20	67.10	21.57	67.07	72.72
2.00	1.80	6.151	448.63	622.66	68.90	20.92	67.33	73.48
0.50	1.90	6.558	478.88	653.91	69.59	21.97	65.85	73.23
1.00	1.90	6.945	480.36	654.39	76.85	21.98	66.89	74.73
1.50	1.90	7.225	477.09	651.12	81.93	21.87	67.43	75.79
2.00	1.90	7.481	472.07	646.10	85.83	21.70	67.71	76.60
0.50	1.70	3.418	477.87	852.00	25.38	21.00	66.21	68.36
1.00	1.70	3.636	484.03	858.06	28.87	22.10	67.90	70.14
1.50	1.70	3.874	442.70	816.73	30.60	20.72	68.77	71.55
2.00	1.70	3.768	420.73	794.76	31.97	19.98	69.28	72.14
0.50	1.80	3.951	488.24	872.27	30.38	22.58	68.01	71.12
1.00	1.80	4.255	503.82	887.85	34.83	22.77	69.88	73.13
1.50	1.80	4.438	494.71	878.74	37.59	22.46	70.97	74.48
1.50	1.80	4.438	494.71	878.74	37.59	22.46	70.97	74.48
0.50	1.90	4.724	513.88	898.01	38.32	23.11	69.40	73.84
1.00	1.90	5.055	520.08	904.11	42.98	23.32	71.04	75.79
1.50	1.90	5.326	520.01	904.04	46.53	23.31	72.02	77.12
2.00	1.90	5.568	517.01	901.04	49.43	23.21	72.61	78.08

given Mach number, so that the eventual choice of inlet M and S should be made on the basis of the tradeoffs between increased power extraction and electrical efficiency on the one hand, and increased size, heat loss and magnet costs on the other.

At the higher stagnation temperature of PSPEC the variations are less dramatic, but similar behavior is shown in Figure 3, and the variation of enthalpy extraction and efficiency can be observed by reference to Table 1-A. Solid lines connect cases which were run with the constant E-field constraint, and it is interesting to examine the effect of variation of M and S on the enthalpy extraction length. For a single-load device operating at constant E-field the value of dh_o/dr remains constant (since $j_-/\sigma u_- = I_{LOAD}/\dot{m}$). Figure 4 shows the length required for 25% enthalpy extraction as a function of M and S, with values of local electrical efficiency at inlet superimposed. L_{25} is a minimum when M = 1.7, but Fig. 3 confirms that slightly higher inlet Mach number is required for reasonable operation with single load. Figure 3 (dashed curves) and Table 1-B also show the effect of introducing a slight relaxation of the constant E-field constraint; additional cases are presented in which the generator loading is constrained to maintain a constant value of K/K_{opt}. The initial loading in each case is set for E = -12 kV/m, but thereafter the field intensity decreases. Slight increases in extraction ratio and efficiency are achievable at the expense of larger size.

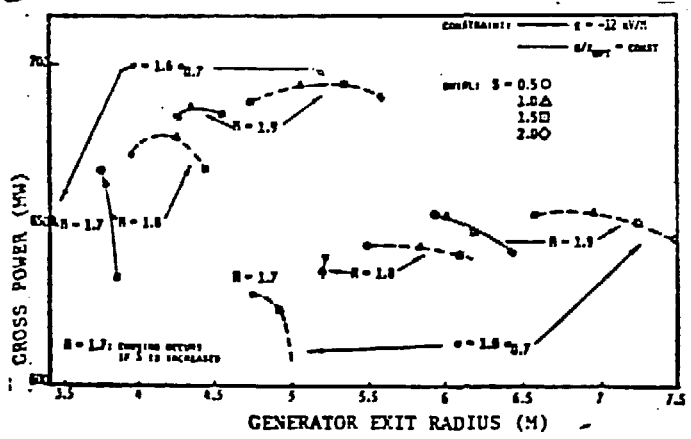

Figure 3. Gross Power vs Exit Radius: Single-load. P_o=8 atm., T_o=2879 K, B=7T, $\sigma/\sigma_{0.7}$=1.0 & 1.6

Unfortunately the off-design performance characteristics of such high power single load devices appear to be unattractive, since the generator tends to operate as a constant current source. Thus some capability for varying the load current in the front or rear of the generator appears essential, and this requirement led to an assessment of the performance of segmented generators with current take-offs at various spacings up to a 1 m separation. The behavior of fluid and electrical properties in one these cases is shown in Figure 5, and the improvements attainable with 0.5 m and 1 m segmentation are shown in Tables 2A and 2B, (using a conductivity enhancement factor of 1.33). The requirement for moderate radial variation of the disk primary load current does not present such severe electrode problems as in a linear generator, and the overall compactness of the symmetric layout and simplified magnet configuration remain as significant attractions. The overall extraction for the Figure 5 case is plotted on Figure 6, taken from Ref. 6. Disk generators designed in this manner are clearly competitive with the equivalent linear channel; the uncertainty range of ~ 2% in enthalpy extraction may still be attributable to discrepancies between Avco and Westinghouse plasma property values.

Table 2. Multiple-load Disk Characteristics.

T_o = 2879 K, P_o = 8 atm., B = 7 T, $\sigma/\sigma_{0.7}$ = 1.33

A. Segmentation Length = 0.52m.

INLET S	INLET M	RMAX (m)	NET P (MW)	POWER (MW)	HT.LOSS (MW)	ENTH. EXTR.	ISEN EFFCY	ELEC EFFCY
0.50	1.80	4.474	492.29	863.32	37.93	22.38	67.25	71.01
1.00	1.80	4.825	504.42	875.45	42.78	22.79	69.21	73.34
1.50	1.80	5.063	505.82	876.85	46.08	22.84	70.15	74.55
2.00	1.80	5.258	501.94	872.97	48.68	22.71	70.58	75.21
0.50	1.90	5.374	507.98	881.89	47.78	22.91	68.68	74.24
1.00	1.90	5.742	517.54	891.57	52.76	23.23	70.27	76.36
1.50	1.90	6.044	518.78	892.81	56.77	23.27	71.07	77.63
2.00	1.90	6.288	515.53	889.56	60.01	23.18	71.44	78.42

B. Segmentation Length = 1.0m.

0.50	1.80	4.470	490.80	864.83	38.17	22.33	67.13	70.89
1.00	1.80	4.736	499.03	873.06	42.36	22.61	68.86	72.81
1.50	1.80	4.985	497.58	873.59	45.80	22.63	69.80	74.00
2.00	1.80	5.169	495.84	869.87	48.22	22.50	70.28	74.74
0.50	1.90	5.300	505.77	879.80	47.28	22.84	68.46	73.64
1.00	1.90	5.594	513.81	887.84	51.73	23.11	69.99	75.74
1.50	1.90	5.862	514.39	888.42	55.48	23.13	70.80	76.87
2.00	1.90	6.114	511.05	885.08	58.78	23.01	71.21	77.80

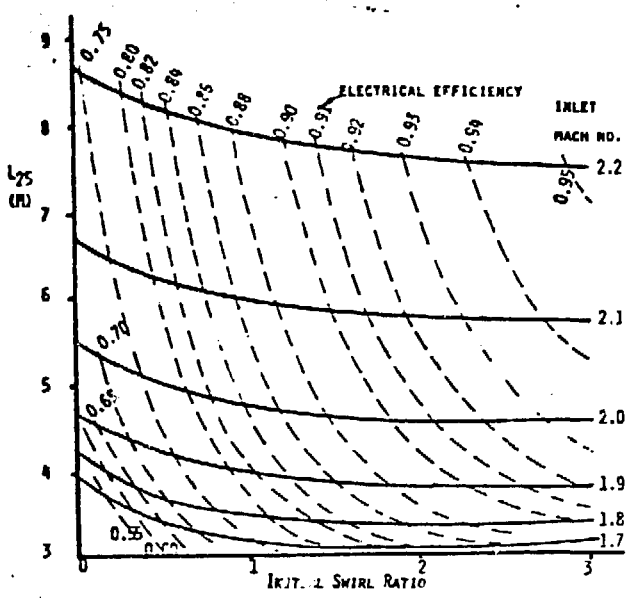

Figure 4. Enthalpy Extraction Length (25% extraction) vs Initial Swirl Ratio. P_o=8 atm., T_o=2879 K, B=7 T, E=-12 kV/m, $\sigma=1.33\sigma_{0.7}$.

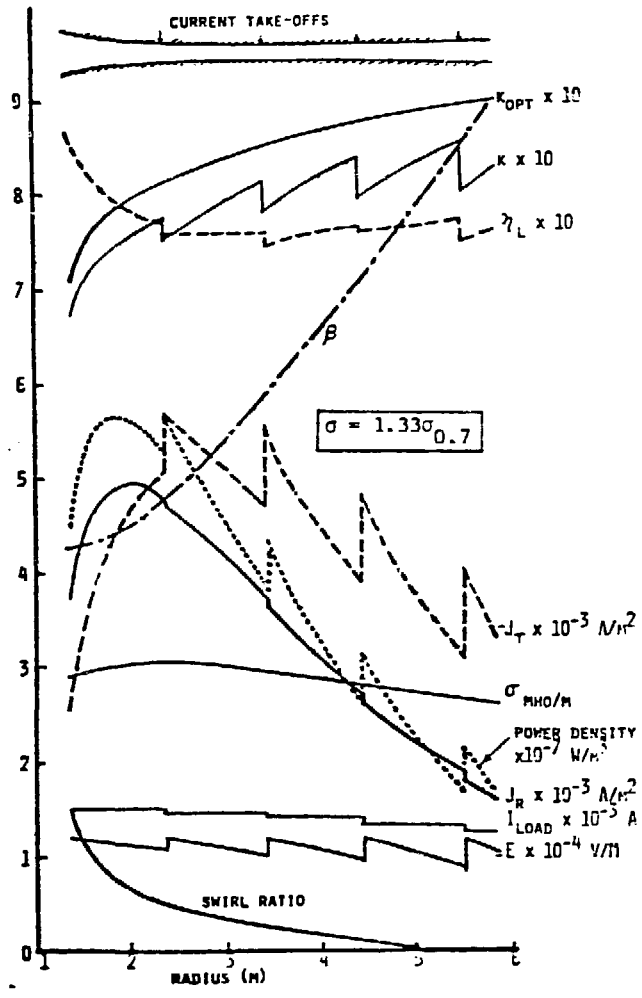

Figure 5. Electrical Behavior of Segmented Disk. Inlet: P_o=7.8 atm., T_o=2879 K, M=1.9.

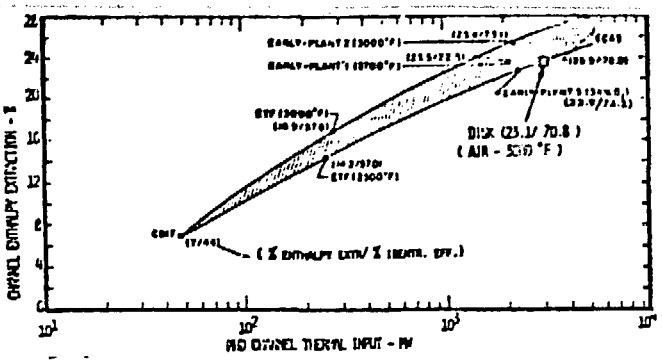

Figure 6. Channel Enthalpy Extraction and Isentropic Efficiency vs Thermal Input (from Ref. 6).

III. Closed-Cycle Disk Generator Optimization

Generator Model Assumptions/Formulation

The two-temperature generator model assumptions and formulation are as follows. The CCD working fluid is cesium-seeded argon. The channel flow is quasi-one-dimensional and accounts for friction and wall heat losses (similar to the OCD model). Finite-rate electron kinetics and energetics are included for analysis of the ionization relaxation processes at the generator inlet and for the cases where the seed becomes fully ionized.[8] The effective conductivity and Hall parameter are determined from reduction formulae developed by Louis.[9] These formulae (which are comparable to those used in linear ECAS studies[10,11]) are applicable for near isotropic turbulence and express the effective properties in terms of the ideal values and a plasma turbulence parameter. The effects of molecular impurities or contaminants are incorporated in the model, with separate collisional loss factors for each species (required to more fully model the recombination rate constants and energy averaged collision frequency). Cross-section data given by Spencer and Phelps[12] are used.

The model formulation consists of solving six conservation equations (three for heavy gas particles and three for the electron species). In addition, a constraint equation, the equation of state, and Ohm's Law are required to solve for the nine dependent variables: n, Ne, U_R, U_θ, E_R, T_{gas}, T_e, p, z; that is, the neutral gas and electron density, radial and azimuthal gas velocity, electric field, heavy gas and electron temperature, pressure and channel height. The constraint equation is handled by requiring the generator to operate, at each radial position, at the local maximum electrical efficiency. Operation close to maximum efficiency is particularly important for closed cycle generators, since the performance is limited primarily by the effective Hall parameter, β_e, rather than by the Hall field constraint (as is the case for OCD). Ionization instabilities which lead to plasma turbulence are minimal in OCD generators, but must be considered in the nonequilibrium case.

Since there is a close coupling and interaction between the generator suboptimization and the system constraints, a simplified argon and steam loop cycle is incorporated in the model. The system includes pressure losses for the generator, nozzle, diffuser and heat exchangers; Table 3 gives the efficiencies for the argon and steam loop components used. The generator heat loss is neglected since it is assumed that the channel walls operate at the adiabatic recovery temperature. The heat source loop is handled by the assumption of a heat source efficiency (of 88%), and air compressor and feed pump work are assumed to be about 5% of the argon compressor work. The system is used primarily to establish the "match" point location relative to the generator exit conditions. This is discussed more fully below.

Table 3. System Parameters for Simplified Cycle Model.

Pressure Losses:	
Diffuser Pressure Ratio (subsonic after inlet shock loss)	.927 (C_p=.8)
Loss between diffuser and compressor	3.0 %
Loss between compressor and nozzle	3.0 %
Efficiencies:	
Adiabatic Nozzle	.99
Compressors	.90
Heat Source (Atmos. Combustion)	.88
Steam Plant (3500/1000/1000)	.42
Temperatures (K):	
MHD Generator Inlet	1920
MHD Generator Exit, T_{oe}	~1250 (Approx)
Argon Compressor Inlet	311
Argon Compressor Outlet, T_{oc}	~ 650 (Approx)
Steam Plant Minimum Temperature	390

Local Performance Characteristics

Relative to open cycle, the CCD generator suboptimization is more complex. In OCD for given stagnation conditions (T_o, P_o), magnetic field, B, and seed fraction, x, the effective transport properties, σ_e and β_e, are uniquely determined by the Mach number, M, and swirl, S; the loading, K, is determined by the additional specification of the current. In the closed-cycle case the electron temperature, T_e, is an additional variable, and the plasma turbulence level, S and the impurity level are additional parameters. Since the generator operates at high interaction, the effective properties depend strongly on the electron temperature and density; the electron mobility (and hence β) is dominated by coulombic collisions. The channel design/shape is extremely sensitive to changes in Ne, and hence the seed fraction (which can be used to control the interaction level) becomes an important parameter in the suboptimization as well. The local load factor also depends on Ne (or Te).

Local performance characteristics for a typical base load CCD are illustrated in Figures 7-9, for stagnation conditions T_o = 1920 K, P_o = 9.0 atm, B = 4.5 T, x = 0.3% and S = 0.2. Figure 7 shows the maximum electrical efficiency as a function of total Mach number, M, for three values of swirl. In general, the efficiency increases with swirl, S, (as expected); at high values of S the efficiency is less sensitive to Mach number. For moderate values (e.g. S = 0.5) the efficiency falls rapidly with increasing M. These results are a consequence of the interaction level achieved in the generator. As M increases, for a given S, the interaction (see Figure 8) increases. When the interaction is high (e.g. S = 0.5 for these conditions) the Hall parameter, shown in Figure 9, is coulomb-dominated and decreases as M and Ne increase. For a lower interaction (e.g. S = 2.0 for these conditions) the Hall parameter is partially controlled by the electron density and partially by the pressure (inverse); the two effects tend to offset one another as M increases and the pressure falls. The latter effect predominates in the OCD generator.

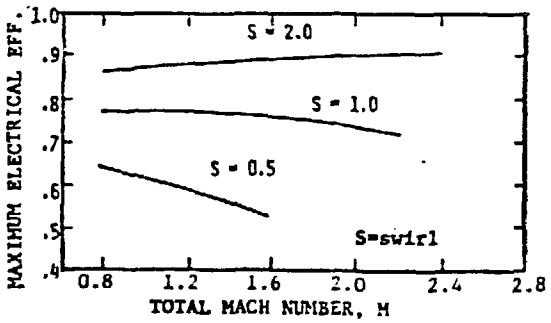

Figure 7. CCD Performance: Maximum Electrical Efficiency vs Mach Number. P_o=9.0 atm., T_o=1920 K, B=4.5 T, x=0.3% Cs, S=0.2, K=K_{opt}.

The enthalpy extraction length, Le, is shown in Figure 8. Le is a measure of the generator length for a given extraction $\Delta h_o/h_o$. Two aspects of the figure are noteworthy. First, there is no minimum value of Le (or optimum M) as is the case for OCD generators, where the conductivity falls off with decreasing gas temperature (see Figure 4, and further examples in Reference 3). Second, Le increases rapidly with S at a given M, since the interaction (i.e.,Ne) decreases with swirl. The opposite behavior occurs in OCD where, for a given M, Le decreases slightly with S (since σ and β are fixed by M, while Le is inversely proportional to the maximum electrical efficiency when K = K_{opt}). These results suggest that, for closed-cycle, the efficiency advantage of high swirl is offset to some degree by an increased extraction length unless the inlet Mach number is relatively high (in the range $2 \leq M \leq 3$). This, however, may not be of consequence since the interaction length for CCD generators is short relative to both OCD and linear generators. The tradeoff can only be assessed by detailed suboptimization calculations integrated

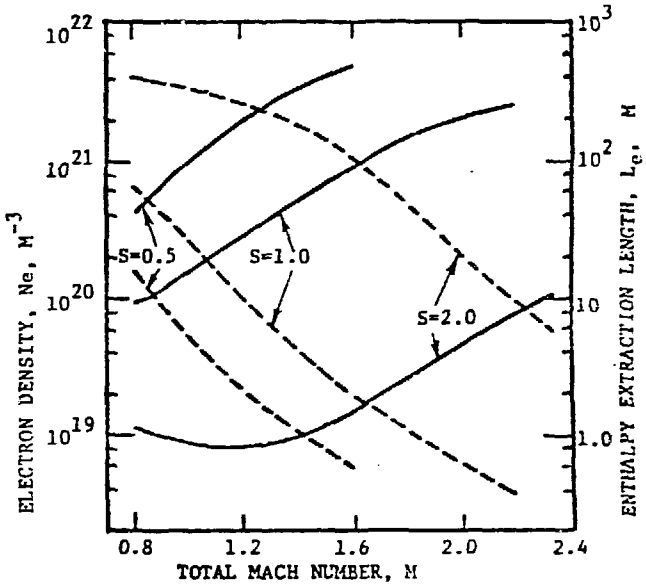

Figure 8. Electron Density (solid lines) and Enthalpy Extraction Length (dashed lines) versus Mach Number for conditions of Figure 7: $L_e^{-1} = dh_o/h_o dr$.

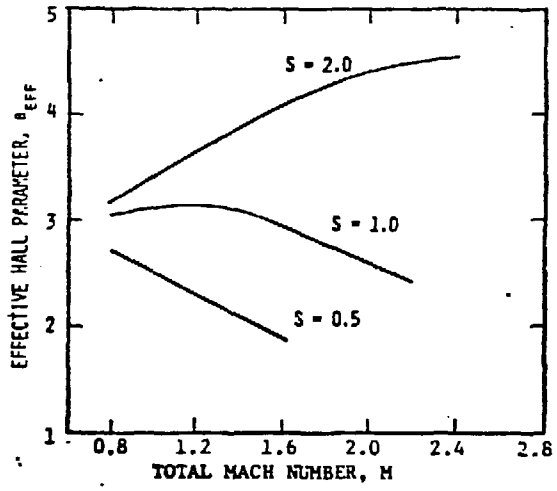

Figure 9. Effective Hall Parameter vs Mach Number for conditions of Figure 7.

with the cycle parameters. The Hall fields developed for these conditions does not exceed 5 kV/m.

Suboptimization Procedure

The generator suboptimization for this study is carried out as follows. The channel is designed for a single load with operation at the local maximum electrical efficiency. The magnetic field and inlet stagnation temperature are constant (6 T, 1920 K). Two plasma turbulence levels are considered, $\hat{S}$ = 0.2 and 0.5, and an impurity level of 18 ppm CO_2 (δ = 2500) and 82 ppm of CO + N_2 (δ = 230) is used for most cases. $\hat{S}$ is defined as the mean square deviation of the fluctuations. The effective Hall coefficient is limited to values of $\beta_{eff} \leq 5$. This imposed constraint is consistent (1) with small-scale laboratory measurements for cases where the seed is near full ionization,[2] and (2) with the linear closed-cycle GE 102, 102A calculations and results[11] for low turbulence ($\hat{S}$ = 0.2).

The stagnation pressure and inlet swirl are varied in the ranges $4 \leq p_o$ (atm) ≤ 12 and $1.0 \leq S \leq 4.0$, respectively. For each combination of p_o, S the inlet Mach number and seed fraction are optimized to yield an exit Mach number in the range 1.0 to 1.1 and a generator pressure ratio which enables operation of the cycle at the match point. The match point is defined as the operating point where the bottoming plant power output is fully utilized to drive the argon cycle and air compressors. The match point efficiency does not necessarily correspond to the maximum system efficiency, since generator turbine efficiency and enthalpy extraction can increase beyond this point. Operation beyond the match point, however, introduces cycle complexities primarily as a result of the requirement that the compressor be partially driven electrically. The match point is determined (in the simplified cycle model) by equating the compressor and bottoming plant shaft work, i.e. $1.05\ (T_{oc} - 311) = 0.42\ (T_{oe} - 390)$. The model closely represents a more detailed (but not fully optimized) systems analysis carried out by Stella[3] for a unit size of 1000 MW_e (case #14, Table 4). Application to other conditions, however, has not as yet been verified, and the results for other unit sizes must be considered as preliminary and approximate. To fully optimize the plant efficiency, a more refined systems model must be coupled to the generator calculations (see discussion below.)

Results

Table 4 summarizes the optimized CCD cases calculated to date. The results shown are S, P_r, M, x, β_e, E.F., η_C, $\eta_{G\&D}$, η_s, L, T_{oc}, F_{comp}, R_o and P which are the swirl, stagnation pressure, total Mach number, seed fraction, effective Hall coefficient (mid-channel), enthalpy extraction, generator turbine efficiency, isentropic efficiency of the generator plus diffuser, system efficiency, interaction length, generator pressure ratio, argon compressor pressure ratio, generator inlet radius, and gross MHD power. The system efficiency is calculated by

$$\eta_s = 0.985\ P\ (0.88)/(\dot{m}\ C_p)_{argon}\ (1920 - T_{oc})$$

where 0.985 is the assumed inverter efficiency. Although coal drying to a 5% moisture level is considered, transformer losses, coal handling, seed processing, etc. are not included. These parasitic losses, however, would be offset to some degree by the improved optimization afforded by a more detailed systems model. Several noteworthy observations are revealed in the table. (1) Turbine and system efficiencies are comparable to those predicted for OCD generators and with those calculated for linear closed cycle channels (which have an interaction length of 10 meters or more).[11] (2) Relatively short interaction and more efficient diffuser configurations are calculated (C_p = 0.8 may be justifiable when guide vanes are used to insure that the boundary layer remains attached). (3) The benefits of inlet swirl are apparent; an average increase of one percentage point in system efficiency is achieved for a ΔS increase of ~ 0.5 (as noted from the $\hat{S}$ = 0.2 results). (4) The inlet Mach number is generally high (M ~ 2-3), consistent with the local performance characteristics discussed above. (5) Higher seed fractions are required at the higher values of swirl (since the interaction level decreases with swirl) in order to constrain the Hall parameter to values less than five. For $\hat{S}$ = 0.2, values of swirl much above two require seeding levels of 1% or more. (6) The interaction length increases and the efficiency decreases with increasing stagnation pressure. (7) Both the interaction and efficiency increase with inlet radius. For these calculations, the inlet channel height is 0.5 meters. The criterion assumed for OCD ($H_i \sim 1/3\ R_o$) is not used here since the interaction length is relatively short. (8) To obtain comparable efficiencies at higher turbulence levels ($\beta_e \sim 2.3$), higher values of swirl and Mach number are required. Excellent performance is achieved at low power levels; however, for large unit size (~ 1000 MW_e) it is clear that parallel generators would be required. (9) The effect of additional impurities is to modify the generator design and operating conditions; however, comparable efficiencies are achievable even when the level is increased from 100 ppm to 200 ppm.

Two examples of the channel design and property profiles are given in Figures 10-15. In Figures 10-12, *case #22 from Table 4 ($\hat{S}$ = 0.2) is shown.* The operating conditions and resulting channel geometry are given in Figure 10. The generator is drawn to scale; other components (dashed lines) are conceptual/schematic. As a result of the high interaction, the generator is relatively short (L/D = 2.0); two-dimensional electrical effects are important and would most likely require a cathode (e.g., tungsten rods) distributed across the exit plane of the channel. To insure a more uniform magnetic field, the split-pair magnet configuration would be preferred, with the cathode located in the vicinity of zero field. The anode can also be divided, as indicated in the figure, or the option of a central rod could be used. The latter affords the possiblitiy of rotation or axial feeding (arc distribution and/or replenishment). The electrical and transport properties for this channel are shown in Figure 11. Near the end of the generator the seed is over 80% ionized. The local power density is denoted as P_D in the figure. The gas properties for this case are given in Figure 12.

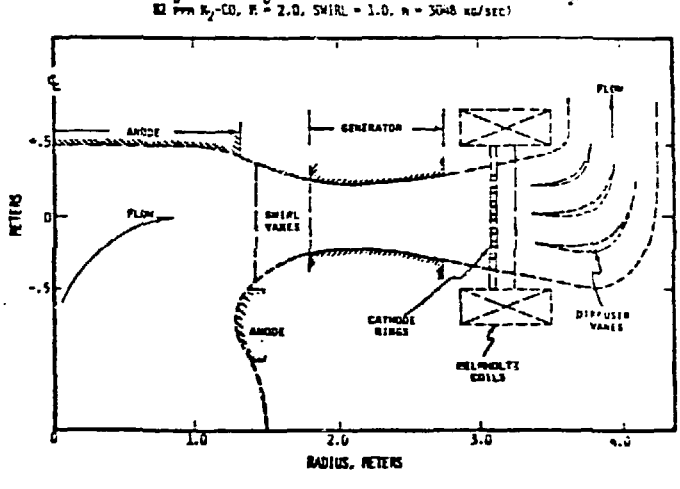

Figure 10. CCD Channel Design - Table 4, Case #22.

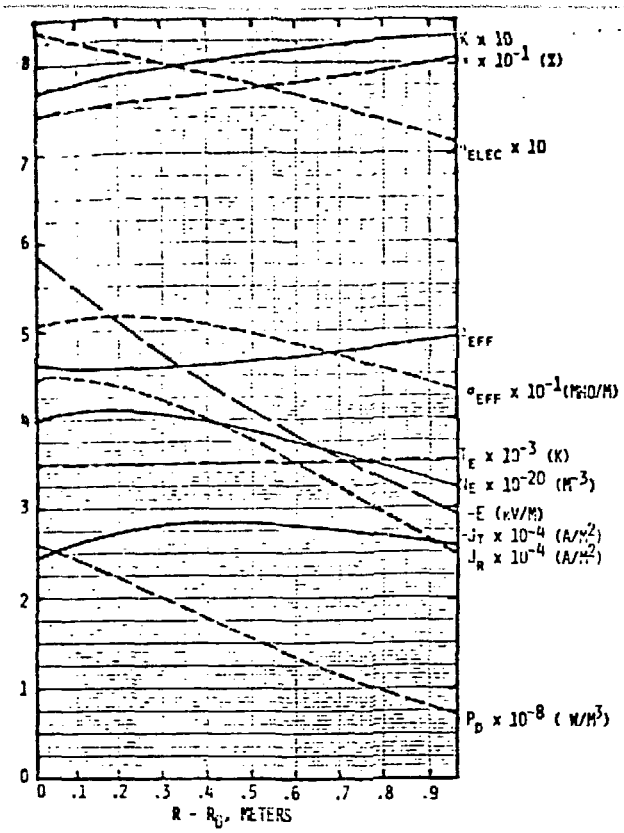

Figure 11. Electrical and Effective Transport Properties for the Generator shown in Figure 10 ($2.06 \leq L_e \leq 2.72$, I=251 kA).

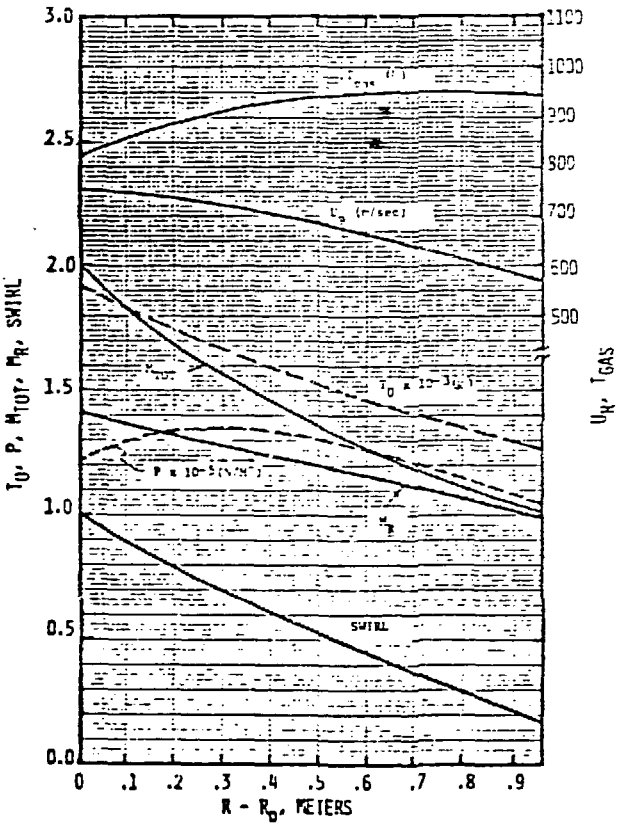

Figure 12. Fluid Property Profiles for the Generator shown in Figure 10. ($\dot{m}$=3048 kg/sec).

Generator designs for the high turbulence assumption are shown in Figures 13-15. The channels are strongly convergent relative to the $\hat{S}$ = 0.2 cases as a result of the high swirl and lower interaction (compare Ne profiles). The current load factor K = K_{opt} is reduced, and the generators operate near maximum power (K = 0.5) as well as maximum efficiency. In addition to generating high inlet swirl, some deswirling is required at the channel exit (see Figure 15). The operation more closely resembles the reaction mode; the radial Mach number is nearly constant and subsonic. An adverse pressure gradient exists in the channel, and boundary layer separation may be a problem which should be assessed.

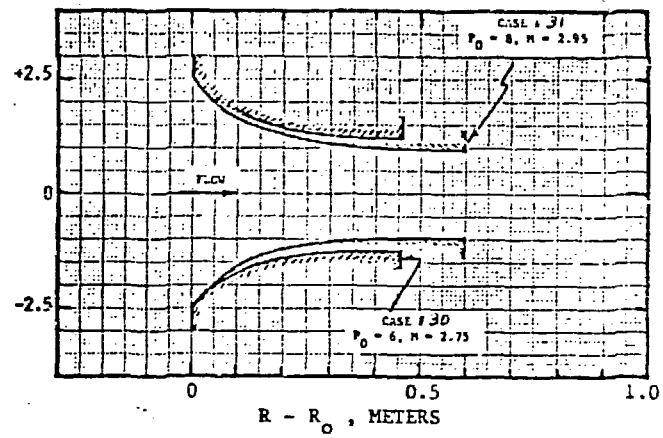

Figure 13. Example CCD Generator Designs for High Plasma Turbulence ($\hat{S}$=0.5).

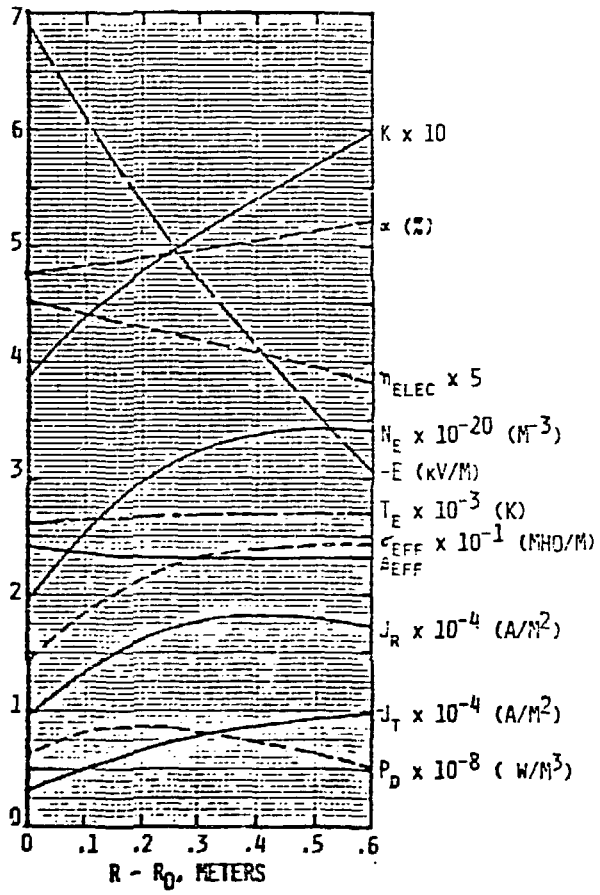

Figure 14. Electrical and Effective Transport Properties for the P_O=8 atm. Generator shown in Figure 13. ($1.23 \leq L_e \leq 1.84$, I=41.7 kA).

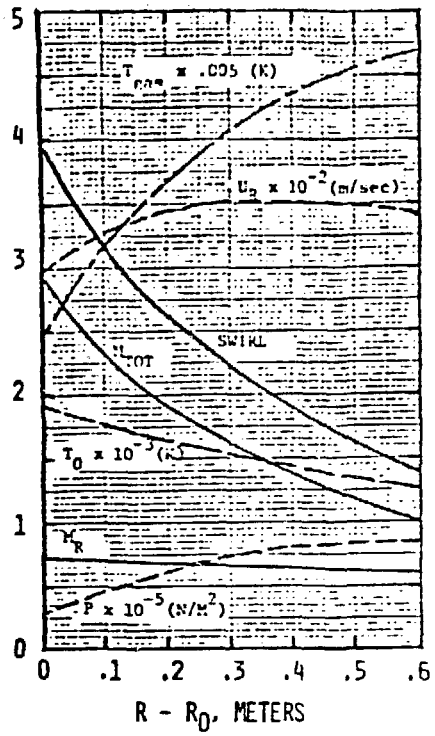

Figure 15. Fluid Property Profiles for the P_0=8 atm. Generator shown in Figure 13. ($\dot{m}$=370 kg/sec).

Figure 16 shows the gross enthalpy extraction versus the turbine efficiency of the combined generator plus diffuser for the cases given in Table 4. The ⊠ data of G.E. are taken from Reference 11; however, the extraction was calculated (using the same definition as MIT) based on the temperatures given in the paper. The comparison shows that the disk achieves about a four point gain in turbine efficiency for the same enthalpy extraction. This suggests that the CCD will have higher cycle efficiencies (by about 1-1.5 percentage points) than the linear Faraday generator when similar system assumptions are used. This is to be expected since the disk can operate with swirl (circular equivalent of a linear diagonal generator), has less friction effects, and a more efficient diffuser. The diffuser recovery is primarily subsonic with a pressure ratio of 0.927 for C_p = 0.8. The inlet shock is weak since the entrance Me is only slightly greater than unity. In addition, the assumption of an adiabatic diffuser for CCD is more realistic than for the linear channel where diffuser lengths are of the order of 20 meters and T_0 ~ 1200 K. The generator + diffuser pressure ratio is shown in Figure 17. Lower ratios (and hence less compressor work) are found for the disk, consistent with the higher isentropic efficiencies (for the same enthalpy extraction).

Figure 18 shows the system efficiency versus turbine efficiency for the disk data relative to the G.E. data. The G.E. results for pressurized combustion with gasifier are taken from Reference 14. The disk data compare favorably with the linear calculations, and reflect the higher turbine efficiency for the disk. From the slopes of the groups of data plotted in Figure 18 it may be seen that a four percent increase in isentropic efficiency yields a 1-1.5 point gain in plant efficiency, consistent with the results presented in Figure 16. For atmospheric combustion the disk data are indeed 1-1.5 points higher than the linear result. A more detailed systems model must be coupled to the generator calculations in order to fully optimize the plant efficiency. The enhanced efficiency, however, would be partially offset by the parasitic losses (mentioned above) not accounted for in the simplified cycle model.

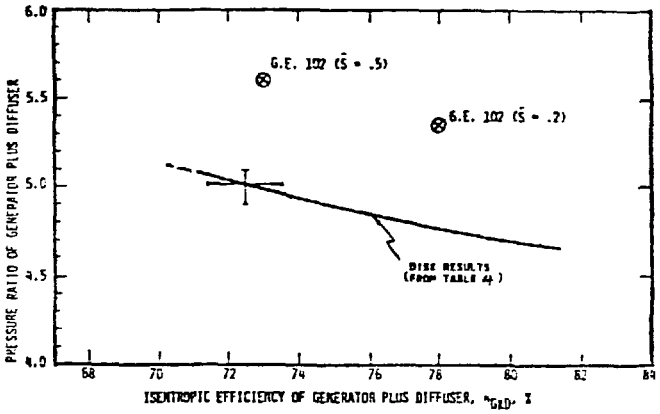

Figure 17. Pressure Ratio Versus Turbine Efficiency of Generator Plus Diffuser.

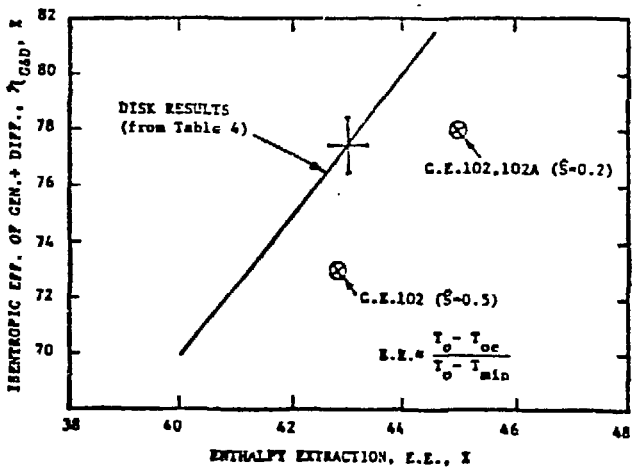

Figure 16. Enthalpy Extraction Versus Turbine Efficiency of Generator Plus Diffuser.

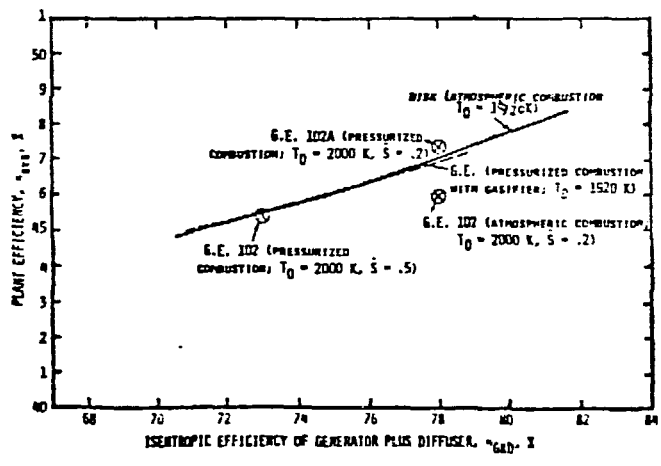

Figure 18. Preliminary Comparison of Closed-Cycle Disk and Linear Systems.

Table 4. Summary of Optimized CCD Cases: Operation at Match Point.

#	S	P_o (Atm)	M	χ	β_e	E.E. (%)	η_G (%)	η_{GAD} (%)	η_s (%)	L (M)	p^r_G	p^r_{COMP}	R_o (M)	P^e (MW)
$\hat{S}$ = .2														
1	2	4	2.02	.135	4.8	44.6	84.3	81.2	48.3	.31	4.33	5.31	1.5	392
2		4	2.02	.405	4.5	44.2	83.6	80.6	48.1	.29	4.33	5.31	3.0	471
3		6	2.22	.135	4.7	44.1	82.7	79.7	47.8	.50	4.41	5.45	2.1	435
4		8	2.25	.405	4.3	42.9	80.5	77.7	47.0	.88	4.41	5.45	3.0	775
5		10	2.50	.100	4.7	42.6	79.9	77.0	46.7	.93	4.40	5.51	2.5	679
6	1.5	6	2.00	.035	4.6	42.8	79.8	77.0	46.9	.37	4.45	5.45	1.5	426
7			2.08	.015	4.8	42.6	79.8	77.0	46.9	.44	4.40	5.41	1.5	409
8			1.95	.045	4.6	43.0	80.4	77.5	47.1	.38	4.45	5.42	2.5	738
9			2.01	.015	4.9	43.2	80.8	77.9	47.2	.52	4.43	5.44	2.5	713
10		8	2.26	.037	4.9	42.1	78.0	75.2	46.2	.81	4.51	5.59	1.5	471
11			2.05	.035	4.7	42.9	79.9	77.1	47.0	.63	4.46	5.48	3.0	1103
12			2.10	.015	4.9	42.8	79.9	77.1	46.9	.78	4.45	5.48	3.0	1065
13		10	2.20	.045	4.5	41.8	77.4	74.7	46.1	.67	4.51	5.58	1.5	608
14			2.13		4.6	42.4	78.6	75.9	46.5	.83	4.51	5.56	2.5	1078
15		12	2.30		4.4	41.5	76.3	73.6	45.6	.84	4.59	5.69	1.5	677
16			2.25		4.5	41.7	77.2	74.5	46.1	.97	4.54	5.59	2.2	1034
17			2.21		4.6	41.8	77.5	74.8	46.5	1.12	4.53	5.56	2.5	1210
18	1.0	8	1.95	.005	4.8	40.7	74.0	71.5	45.1	.83	4.68	5.73	1.5	711
19			1.93		4.8	40.9	74.5	71.9	45.2	.85	4.67	5.71	1.8	868
20			1.91		4.8	41.1	75.0	72.4	45.4	.87	4.66	5.70	2.2	1050
21		10	2.05		4.7	40.3	72.9	70.5	44.7	.89	4.75	5.83	1.5	826
22			2.00		4.6	40.3	73.5	71.0	44.9	.96	4.68	5.74	1.8	1025
23			2.00		4.7	40.6	73.7	71.2	45.0	.97	4.70	5.77	2.0	1146
24			1.98		4.7	40.7	73.9	71.5	45.0	1.00	4.69	5.76	2.2	1270
25			2.00		4.7	40.8	74.2	71.7	45.1	.95	4.68	5.74	2.5	1438
26		12	2.10		4.6	40.0	71.9	69.5	44.3	1.05	4.80	5.90	1.5	945
27			2.02		4.6	40.4	73.3	70.8	44.8	1.22	4.71	5.78	2.5	1688
$\hat{S}$ = .5														
28	4.0	4	2.35	.300	2.4	43.0	80.9	78.0	47.1	.43	4.39	5.45	2.5	164
29			2.35		2.4	42.9	81.1	78.2	47.1	.42	4.34	5.40	3.0	197
30		6	2.75		2.3	41.4	77.1	74.3	45.6	.46	4.47	5.65	1.5	108
31		8	2.95	.100	2.3	40.2	74.7	70.5	44.7	.60	4.52	5.78	1.5	124
32		10	3.02		2.3	39.5	73.1	70.6	44.1	.92	4.55	5.84	2.5	241
(200 ppm Impurities; $\hat{S}$ = .2)														
33	2	8	2.50	.405	4.4	42.0	78.7	75.9	46.3	1.14	4.43	5.54	2.5	534

IV. Conclusions

An open-cycle disk generator appears capable of yielding over 23% enthalpy extraction at 71% isentropic efficiency when supplied with plasma conditions similar to those assumed in the Avco PSPEC study. This performance is achieved by slight radial variation of the load current to maintain adequately high enthalpy extraction rate and electrical efficiency. Since some current take-off electrodes would be essential for off-design operation, this segmenting of the device is not expected to be a major drawback. The study confirms that the disk configuration could provide a viable MHD generator for open-cycle base-load power generation.

The closed-cycle disk is characterized as a short (L ~ 1.0 meter and diffuser ~ 1-2 meters), compact and efficient generator. The results of this initial study strongly indicate that the CCD MHD/steam power plant is competitive with both closed-cycle linear and open-cycle systems. However, a full optimization of the integrated system with a more refined analysis is needed. In addition, conceptual design and costing studies are required to complete the assessment of the maximum potential of a CCD power plant.

Acknowledgments

The authors gratefully acknowledge the technical support and assistance given by Messrs. M. Stella of the Westinghouse AESD, B. Misra of M.I.T., and D. Chubb of NASA LeRC. The work was partially supported under NASA Contract DEN3-139 through a subcontract with Westinghouse Advanced Energy Systems Division.

References

1. Louis, J.F. AIAA J., 6, 1674(1968)
2. Loubsky, W.J, V.J. Hruby, and J.F. Louis, Proc. of 15th Symp. on Eng. Aspects of MHD, VI.4, 1976.
3. Nakamura, T., and M.K. Jenkins, Proc. of 18th Sym. on Eng. Aspects of MHD, B.3.1. 1979.
4. Klepeis, J.E. and V.J. Hruby, Addendum paper at 16th Symp. on Eng. Aspects of MHD, 1977.
5. Shioda, S., et al, Proc. of 18th Symp. on Eng. Aspects of MHD, D-2.6.1, 1979.
6. Hals, F.A., "Parametric Study of Potential Early Commercial MHD Power Plants," NASA CR-159633, Dec, 1979.
7. Coderre, W.J., "Coal-fired Open Cycle MHD Combustion Plasmas: Chemical Equilibrium and Transport Properties Workshop Results," AIAA Paper 80-0091, Jan, 1980.
8. Lytle, J.K., W. Loubsky, M. Rosenbaum and J.F. Louis, Proc. of 18th Symp. on Eng. Aspects of MHD, D-2.5.1, 1979.
9. Louis, J.F., Proc. of 8th Symp. on Eng. Aspects of MHD, 1967.
10. General Electric Phase I Final Report; Energy Conversion Alternative Study (ECAS), NASA CR 134948, Feb. 1976.
11. Zauderer, B., Proc. of 15th Symp. on Eng. Aspects of MHD, II.5, 1976.
12. Spencer, F.E., Jr. and A.V. Phelps, Proc. of 15th Symp. on Eng. Aspects of MHD, III.5, 1976.
13. Stella, M., (private communication) Westinghouse AESD, Large, PA, 1980.
14. Marston, C.H., et al, Proc. of 16th Symp. on Eng. Aspects of MHD, X.5.29, 1977.